

Benchmarking of density functionals for Z-azoarene half-lives via automated transition state search

Author list: Daniel M. Adrion, Danil Kaliakin,[‡] Patrick Neal,[‡] Steven A. Lopez*

Affiliations: Department of Chemistry and Chemical Biology, Northeastern University, Boston, Massachusetts, 02115, United States

Corresponding author: s.lopez@northeastern.edu

[‡]Authors contributed equally to this manuscript

Abstract

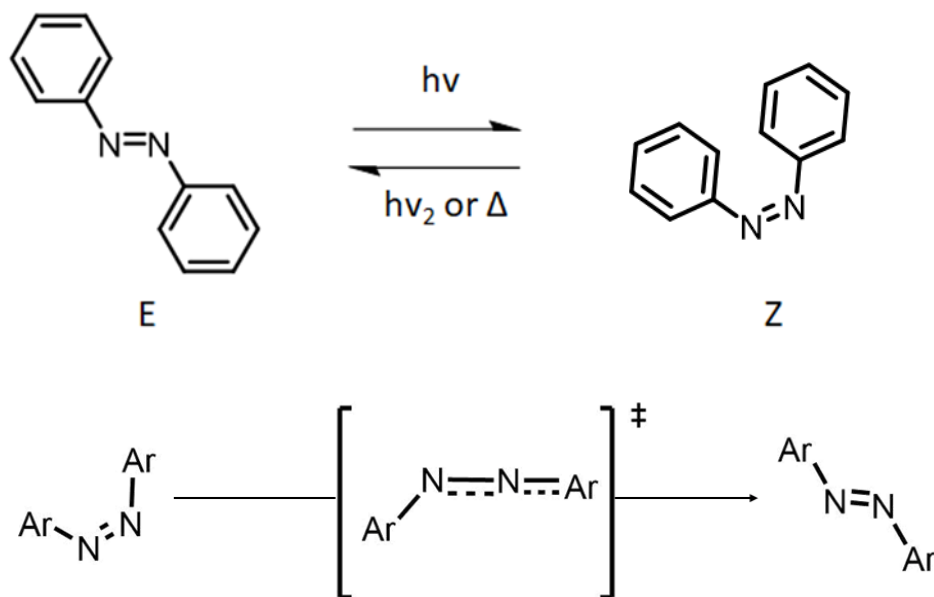
Molecular photoswitches use light to interconvert from a thermodynamically stable isomer into a meta-stable isomer. Chemists and materials scientists have applied photoswitches in photopharmacology, catalysis, and molecular solar thermal (MOST) materials. Visible-light-absorbing photoswitches are attractive because the relatively low-energy light minimizes undesired photochemical reactions and enables biological applications. Designing ideal photoswitches requires long-lived metastable states; predicting their half-lives with theory is difficult because it requires locating transition structures. We now report the *EZ*-TS code, which automates the prediction of rate constants for the thermal $Z \rightarrow E$ isomerization. We leverage *EZ*-TS to automate the location of the favored transition structure and to comprehensively benchmark the performance of 140 model chemistries against the experimental rate constants of 11 azoarenes. We used 28 density functionals [local spin density approximation, generalized gradient approximation, meta-GGA, hybrid GGA, hybrid meta-GGA], and five basis sets [6-31G(d), 6-31+G(d,p), 6-311+G(d,p), cc-pvdz, and aug-cc-pvdz]. The hybrid GGA functionals performed the best of all tested functional classes. We demonstrate that the mean absolute errors of 14 model chemistries approach chemical accuracy, and mPWPW91/6-31+G(d,p) achieves chemical accuracy and should be used with *EZ*-TS.

Introduction

Molecular switches are organic or organometallic molecules that cycle between two distinct chemical states when subject to an outside stimulus such as changes in pH,¹⁻⁶ mechanical force,^{7, 8} solvent polarity,⁹ and light.^{10, 11} These two states have distinct chemical and physical properties, accessible by switching the stimulus on or off. Light stimulus is easily controlled spatiotemporally and promotes cycling between two photoswitch states. Azoarene photoswitches contain two aryl groups on either side of an N=N diazo bond, and their switching mechanisms are light-activated. Many classes of photoswitches have emerged in the literature, but azobenzenes are considered prototypical molecular switches because of their relatively straightforward syntheses and reliability. The vast majority of azobenzenes require ultraviolet light to promote photoswitching.¹² The relatively low-energy of visible light generally avoids undesired photochemical reactions, thus broadening the utility of visible-light photoswitches in biological¹³⁻¹⁸ and materials science

applications.¹⁹⁻²¹ Replacing the benzene moiety of azobenzene with heteroaryl groups has resulted in red-shifted absorbance maxima (λ^{\max}) and improved thermal half-lives over azobenzenes. Azoheteroarenes with aryl rings containing nitrogen²²⁻²⁶, sulfur²⁷⁻³⁰, and oxygen³¹ atoms have been studied. Recent studies by Dreuw and Wegner have shown that thiophenylazobenzene molecules exhibit redshifted λ_{\max} values over azobenzene of up to 60 nm, and near quantitative (>95%) photoswitching of the *E* isomer when irradiated with visible light.³² Heindl and Wegner also found in 2020 that substituting the phenyl ring of thiophenylazobenzene with an electron-withdrawing group can stabilize the meta-stable *Z* isomer, and can increase the half-life to up to 17.7 hours.³³ Azofuran molecules are the least explored of our given examples. A study from 2006 conducted by Oliveira et al. found that a diphenyl furan molecule was effective in inhibiting the growth of cancer in human cells.³¹ The photophysical properties of polymer materials containing a diazofuran moiety were investigated in 2005 by Wang et al.³⁴ A diazofuran dye molecule was also included in a study conducted in 2000 by Åstrand et al.³⁵ to investigate the effectiveness of five-membered rings as optical data storage materials. To the best of our knowledge, there have been no studies on the thermal properties of diazofuran molecules to date. Nitrogen-containing photoswitches have by far been the most explored of all heteroaryl photoswitches. These molecules feature improved *Z*-isomer half-lives over azobenzene, ranging from 10 days to 46 years with near-quantitative bidirectional photoswitching (>98% pss).^{22, 23} The design of next-generation photoswitches is challenging because of the simultaneous tuning of multiple performance parameters: 1) λ_{\max} , and the minimal overlap between the absorbance spectrum of the *trans*- and *cis*-isomers, ($\Delta\lambda_{\max}$), 2) the half-life of the relative thermal stability of the metastable isomer ($t_{1/2}$), 3) steady-state relative population of the photostationary states of the stable and meta-stable isomers, and 4) reproducibility of the switching over time. This report provides a new computational tool to predict the $t_{1/2}$ of meta-stable *Z*-isomers; Scheme 1 illustrates the reaction and interconversion transition state that depletes the population of the metastable *Z* isomer (Scheme 1).

Scheme 1. Azobenzene photoswitching and thermal isomerization reaction. Generalized azoarene photoswitch, undergoing $Z \rightarrow E$ isomerization via an inversion mechanism.



Three possible mechanisms have been put forth to describe the thermal back-isomerization: 1) *rotation* about the CNNC dihedral,³⁶ 2) *inversion*—one side of the π_{NN} bond becomes nearly collinear with one of the aryl rings,³⁶ 3) *hula-twist*—the transition structure features a twisting motion about the π_{NN} bond while the aryl groups maintain their relative orientations.³⁷ Density functional theory (DFT) calculations suggest that the inversion mechanism is generally preferred for the $Z \rightarrow E$ thermal isomerization.^{36, 38-40} Rietze and co-workers benchmarked density functionals against experimental ΔG^\ddagger for azobenzene and one azobenzene derivative, AzoBiPyB in 2017.⁴¹ The AzoBiPyB molecule is azobenzene functionalized with pyridines at the *meta* positions of one benzene. This study benchmarked 13 method and 7 basis sets, which includes standard Hartree-Fock calculations, meta-GGA functionals and range separated GGA functionals. The authors concluded that the B3LYP and BMK density functionals with the 6-31G(d) basis set are both predicted ΔG^\ddagger to within ~ 1 kcal mol⁻¹ of experimental values. These studies have shown that the B3LYP functional, coupled with Grimme's dispersion correction D3BJ⁴²⁻⁴⁴ and the 6-31G(d) basis set⁴⁵ provided an acceptable compromise between computational cost and accuracy.^{37, 38, 46}

The limited number of benchmarked model chemistries and molecular scope of azobenzenes has raised doubts on whether B3LYP/6-31G(d) is still the best model chemistry to use. Indeed, there is no guarantee that the performance can be transferred from one molecular class to another. Further, the performance of density functionals cannot be systematically improved. There is no guarantee that utilizing additional terms or basis functions will improve the description of molecular geometries and or energies.⁴⁷ Kohn–Sham (KS)-DFT is formally exact, but it involves an exchange-correlation (xc) functional. The xc functional is referred to as a density functional;

the exact form of this functional is unknown and essentially unknowable. KS theory involves parametrizing the electron density by a Slater determinant, which enforces the Pauli exclusion principle and permits the calculation of non-interacting kinetic energy from the orbitals of the Slater determinant as if it were a wave function. The KS orbitals satisfy a set of coupled differential equations similar to the Hartree-Fock (HF) equations of wave function theory (WFT) but containing the xc potential instead of the HF-exchange potential. The xc potential approximates the exchange and includes electron correlation and the electron kinetic energy beyond the non-interacting part(s). All xc functionals have empirical components; these components are often parameters fitted to experimental data and *ab initio* data and may combine various kinds of empiricism.⁴⁸

Jacob's ladder is an organizational scheme for density functionals with five rungs representing increasing levels of theoretical rigor in xc potentials with higher computational cost.^{47, 49} From lowest to highest, the rungs are local spin density approximation (LSDA) functionals, generalized gradient approximation (GGA) functionals, meta-GGA functionals, hybrid GGA functionals, and generalized random phase approximations (RPA) functional.⁴⁷ Herein, we include functionals from the first four rungs of Jacob's ladder.

Scheme 2. Representation of Jacob's ladder of density functionals.



The local spin-density approximation (LSDA) is the simplest exchange-correlation functionals, which occupy the first rung of Jacob's Ladder. These functionals assume an infinite uniform electron gas; while computationally expedient, these functionals are typically unable to reproduce

experimentally measured molecular properties, since a majority of molecules and materials have inhomogeneous density distributions. Generalized gradient approximation (GGA) functionals improve upon the systematic errors of the LSDA by introducing a factor that partially accounts for inhomogeneous densities. These functionals occupy the second rung of Jacob's Ladder and show significant improvements relative to LSDA. Two additional independent ingredients that further improve the functional's accuracy are the Laplacian of the electron density or the kinetic energy density.⁵⁰ The kinetic energy density describes electron delocalization in π -conjugated molecules.⁵¹ The third rung of Jacob's Ladder and are known as meta-generalized-gradient approximations (meta-GGA); meta-GGA functions include either the Laplacian of the electron density or the kinetic energy.⁴⁷ Despite the improvement offered by Laplacian of the electron density or the kinetic energy, self-interaction error (SIE), long-range dynamic correlation (dispersion), and strong correlation cannot be remedied within LSDA, GGA, and meta-GGA.⁴⁷ In Kohn-Sham (KS)-DFT, since the exact exchange term is replaced by the exchange-correlation functional, most functionals are not one-electron SIE-free.⁵² Leveraging an 'exact' HF-exchange functional with a local correlation functional gives exactly zero correlation energy for one-electron systems has proved effective to improve SIE. Becke pioneered the mixing of a global fraction of exact exchange with the exchange-correlation functional,^{44, 53} which resulted in the solution that defines Rung 4 of Jacob's Ladder (hybrid GGA and hybrid meta-GGA).⁴⁷

Computational Methods

We used 28 density functionals and five different basis sets. The list includes hybrid functionals that include Grimme's empirical dispersion correction (PBE0,⁵⁴ B3LYP,^{44, 55-57} and BMK⁵⁸), the Petersson-Firsch Dispersion correction (APFD),⁵⁹ no dispersion corrections (MN12-SX,⁶⁰ M06-2X,⁶¹ M06-HF,⁶² PBEh1PBE,⁶³ OHSE2PBE,⁶⁴ and mPW1PW91⁶⁵), functionals with long-range corrections (CAM-B3LYP,⁶⁶ ω b97XD,⁶⁷ and LC-wHPBE⁶⁸), functionals with generalized gradient approximations (GGA) (M11L,⁶⁹ N12-SX,⁶⁰ mPW1B95,⁷⁰ mPW1PBE,^{65, 71} TPSS1KCIS,⁷² mPW1B1K,⁷⁰ mPW1K,⁷³ BB1K,⁷⁴ BHandH,^{55, 75} ω B97,⁷⁶ and ω B97X⁷⁶), the τ -corrected gradient correlation functional TPSSH.⁷⁷ and functionals with local spin density approximations (LSDA), (SVWN⁷⁸ and SVWN5^{56, 78}). We have combined the following five basis sets with each density functional: 6-31G(d), 6-31+G(d,p), 6-311+G(d,p),⁴⁵ cc-pvdz, and aug-cc-pvdz.^{79, 80} We included the common double- and triple- Pople family basis sets with and without diffuse functions. We also included correlation consistent basis sets with and without diffuse functions, because they systematically result in smooth convergence of energies toward the complete basis set (CBS) limit with the cardinal number, n (in cc-pVnZ). This feature permits the systematic improvement of *ab initio* energies with basis set size.⁸¹⁻⁸⁴ All optimizations are performed using the Integral Equation Formalism Polarizable Continuum Model⁸⁵ (IEFPCM) for water in Gaussian 16.⁸⁶

Discussion/Results

The purpose of this study is 3-fold: 1) Identify the most accurate model chemistry for predicting the ΔG_{comp}^\ddagger for the thermal reversion reactions of azoarenes, 2) Obtain a clear idea of functional and basis set effects on ΔG_{comp}^\ddagger free energies and thermal isomerization mechanisms, 3) Demonstrate how our open-source *EZ-TS* code can be used to automate thermal isomerization transition structures of diazoarenes. After searching the literature for experimental half-lives and corresponding k_{exp} we identified many more azoarenes than we could benchmark in a single report. We excluded all azoarenes that featured extended alkyl chains,⁸⁷ transition metal complexes,^{88, 89} or macrocycles.⁹⁰⁻⁹² We decided not to include these classes of azoarenes because of the exponentially larger computational cost associated with evaluating the conformational space of alkyl chains and inconsistent performance of density functionals for organometallic species.^{93, 94}

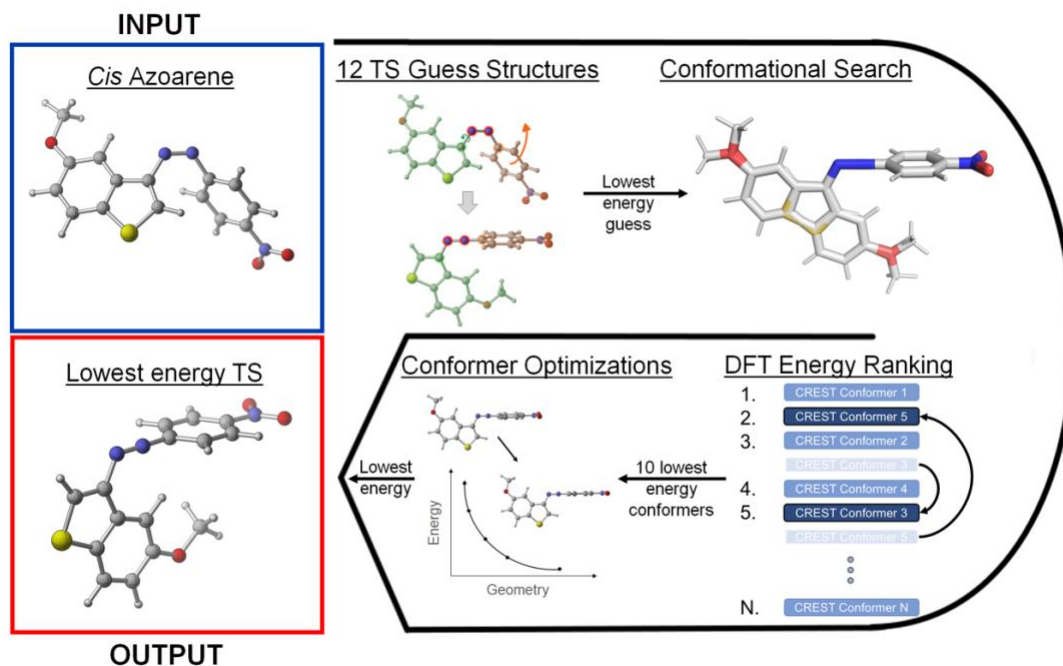
Conformational search of *Z*-isomers

We developed a computational workflow to determine the lowest energy conformer of the reactant (*Z*-isomer) for the thermal back-reaction. The simplified molecular-input line-entry system (SMILES)⁹⁵ string is first read in using openbabel, which generates a rough 3D coordinate file (*e.g.*, .xyz). The coordinate file is passed to the Conformer Rotamer Ensemble Sampling Tool (CREST) tool,⁹⁶ which uses metadynamics simulations to sample the conformational space of organic molecules. A CREST conformational search can yield up to 100 possible conformers. The xTB⁹⁷ minimization procedure led to inaccurate structures that had convergence failures across the wide range of functionals in this report. We introduced a workaround that involved a partial optimization scheme, where each xTB-structure structure was relaxed with 5 B3LYP/6-31G(d) optimization steps using ORCA⁹⁸. The resulting conformers are ranked by energy and the 10 lowest energy conformers are fed into the optimization and vibrational analysis portion of the workflow.

EZ-TS open-access code

EZ-TS leverages molecular dynamics simulations and DFT calculations to locate the lowest energy transition structure for each *Z* → *E* isomerization; this workflow is illustrated in Scheme 3. *EZ-TS* aims to contribute to the growing body of codes meant to automate quantum chemical calculations.⁹⁹⁻¹⁰²

Scheme 3. *EZ-TS* workflow starting from an optimized *cis* geometry (top left) and undergoing conformational searching and optimizations towards the lowest energy transition structure (bottom left).



EZ-TS (available at <https://github.com/lopez-lab>) first generates a 3D input structure as described in the computational methods section. The resulting 3D geometry is automatically altered to generate 12 input guess-structures by setting the CNN angle to a value between 120 and 180°. These input structures are then initially optimized with B3LYP(D3BJ)/6-31G(d); a vibrational analysis is performed to verify that the stationary point is indeed a transition structure (one negative frequency). We observed that the imaginary frequency for the inversion mechanism is typically in the range of -500 - -200cm^{-1} . For the rotation mechanisms, we observed imaginary frequencies in the range of -1000 - -700cm^{-1} . Each of these transition structures is subjected to a CREST conformational search with constrained CNNC dihedral angle and both CNN angles (highlighted in Scheme 3). The truncated optimization scheme is also applied to the transition state conformational search as described above. After this partial optimization, the conformers are ranked by energy, and the 10 lowest conformers are subject to an optimization and vibrational analysis procedure using B3LYP-(D3BJ)/6-31G(d) using the Gaussian16 software. The energies of these 10 TS-conformers are ranked, those transition structures with frequencies not corresponding to azoarene isomerization mechanisms ($>-200\text{cm}^{-1}$) are discarded.

With *EZ-TS* in hand, we used high-performance computing to predict the corresponding thermal rate constants k_{exp} of the 12 azoarenes with 28 density functionals and 5 basis sets; the k_{comp} are compared to experimental k_{exp} . We report deviations of k_{comp} from k_{exp} as mean average

error (MAE) for each combination method and basis set. Scheme 4 shows the 12 tested azoareenes, and their names in the associated references.

Scheme 4. Tested set of 12 azoarene photoswitches. Their labels from the relevant references are given.

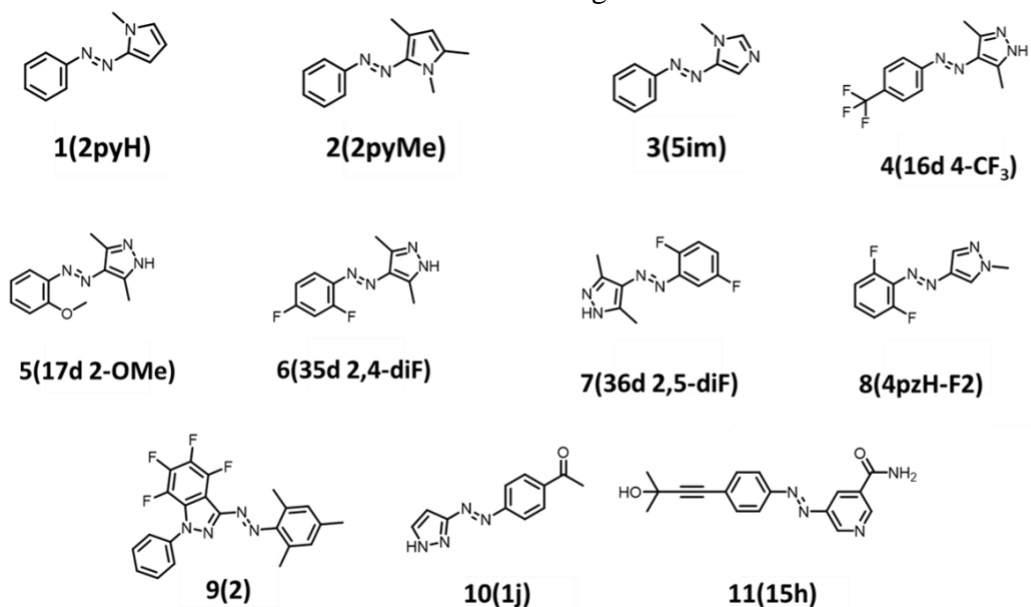


Table 1 shows a summary of the 12 included azoarenes and their corresponding $\Delta G_{\text{expt}}^\ddagger$, k_{expt} , and known reaction conditions (solvent and temperature).

Table 1. List of benchmarked azoarenes and corresponding $\Delta G_{\text{expt}}^\ddagger$ (kcal mol⁻¹), k_{expt} (s⁻¹), and reaction conditions (solvent and temperature).

Mol	Name in Ref	$\Delta G_{\text{expt}}^\ddagger$	k	Conditions
1	2pyH	23.1	6.50×10^{-5}	MeCN 25 °C
2	2pyMe	19.5	3.30×10^{-2}	MeCN 25 °C
3	5im	25.5	1.20×10^{-6}	MeCN 25 °C
4	16d 4-CF ₃	21.9	4.93×10^{-4}	MeCN 25 °C
5	17d 2-OMe	23.9	1.73×10^{-5}	DMSO 25 °C
6	35d 2,4-diF	23.3	5.43×10^{-5}	MeCN 25 °C
7	36d 2,5-diF	20.6	4.72×10^{-3}	DMSO 25 °C
8	4pzH-F2	30.1	4.80×10^{-10}	DMSO 25 °C
9	2	25.6	1.07×10^{-6}	DMSO 25 °C
10	1j	24.3	9.63×10^{-6}	DMSO/H ₂ O
11	15h	25.1	2.50×10^{-6}	MeCN 25 °C

We translated the cited molecule name from the original reference into numbers for clarity. The experimental $\Delta G_{\text{exp}}^\ddagger$ ranges from 19.7 to 30.1 kcal mol⁻¹, spanning 7 orders of magnitude for rate constants. The large range of rate constants supports our claim of a sufficiently diverse set of azoarenes for a benchmarking study. Next, we begin to assess the performance of all included model chemistries on predicting azoarene $Z \rightarrow E$ thermal isomerization barriers.

Overall performance

Figure 1 summarizes the MAEs for $\Delta G_{\text{comp}}^\ddagger$ for each of the 140 model chemistries. The different shapes are organized by basis set; the red shapes correspond to basis sets with diffuse functions (6-31+G(d,p) and aug-cc-pvdz), and the black unfilled shapes correspond to 6-31G(d) (black circles) and cc-pvdz (black triangles). The filled black squares correspond to the 6-311+G(d,p) triple- ζ basis set. The functionals are distributed based on MAE, going from largest to smallest.

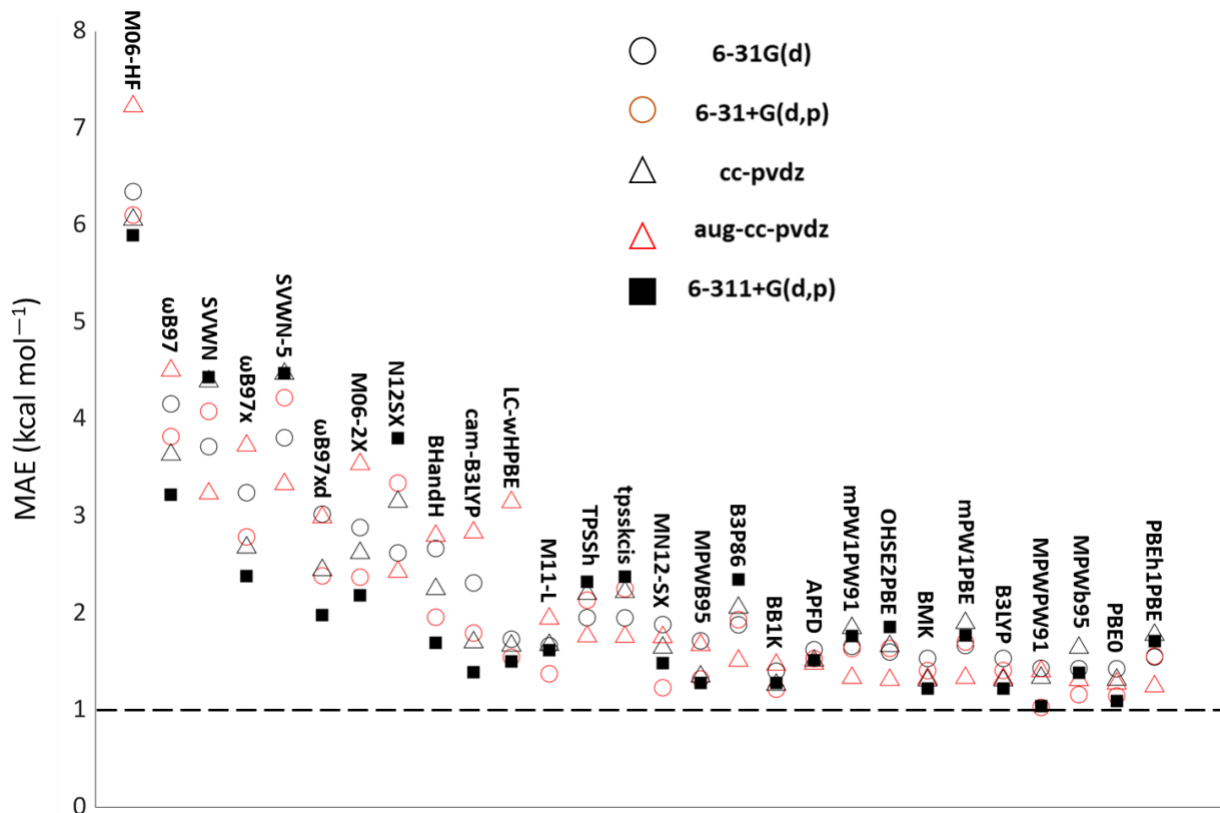


Figure 1. Scatter plot of 140 model chemistries (28 functional and 5 basis set combinations). The 6-31G(d), 6-31+G(d,p), cc-pvdz, aug-cc-pvdz, and 6-311+G(d,p) basis set MAEs are shown as the black circles, red circles, black triangles, red triangles, and black squares, respectively. The dotted black line represents the cutoff of chemical accuracy (1.0 kcal mol⁻¹).

The MAEs across all functionals ranged from 1.0 kcal mol⁻¹ to 7.2 kcal mol⁻¹. The best overall performance was achieved by mPWPW91/6-31+G(d,p) and the worst overall performance was

achieved by M06-HF/aug-cc-pvdz. A visual inspection of the data presented in Figure 1 suggests that the choice of density functional affects MAEs more strongly than the basis set. The MAEs have a relatively narrow range across the five basis sets; the APFD functional yields the smallest range of 0.1 kcal mol⁻¹, while the M06-HF functional affords the largest range (1.6 kcal mol⁻¹). Further, increasing the basis set size from double- ζ (6-31G(d)) to triple- ζ (6-311+G(d,p)) does not affect average MAE (both have an average of 2.2 kcal mol⁻¹). We next analyzed the performance of the density functionals with the 6-311+G(d,p) basis set from high to low MAEs. The 10 worst-performing functionals have MAEs that range from 2.0–5.9 kcal mol⁻¹. The M06-HF functional gave the highest MAEs, significantly higher than the other functionals. The high MAEs of M06-HF are consistent with respect to basis set; the MAEs ranged from a low of 5.9 kcal mol⁻¹ (6-311+G(d,p) basis set) to 7.2 kcal mol⁻¹ (aug-cc-pvdz basis set). After M06-HF, the second-worst model chemistry was SVWN-5/cc-pvdz with an MAE of 4.5 kcal mol⁻¹.

The best-performing functionals show an MAE range of 1.0–1.9 kcal mol⁻¹. These functionals are PBE0, MN12-SX, cam-B3LYP, mPWPW91, mPWB95, B3LYP, OHSE2PBE, mPW1PBE, mPW1PW91, PBEh1PBE, M11-L, LC-wHPBE, MPWb95, BHandH, BMK, BB1K, and APFD. There is also a second tier of functionals, which contains the worse performing ones (MAEs of 2.0 kcal mol⁻¹ and above). The functionals here include SVWN, SVWN-5, M06-2X, M06-HF, N12-SX, B3P86, ω b97, ω b97x, ω b97xD, TPSSh, and tpskcis. Next, we will rationalize these tiers of MAEs across all density functionals. Figure 3 shows the MAE of each density functional used with the 6-311+G(d,p) basis set. We use only this triple- ζ basis set for this analysis, as it afforded the lowest MAE when averaged across all functionals.

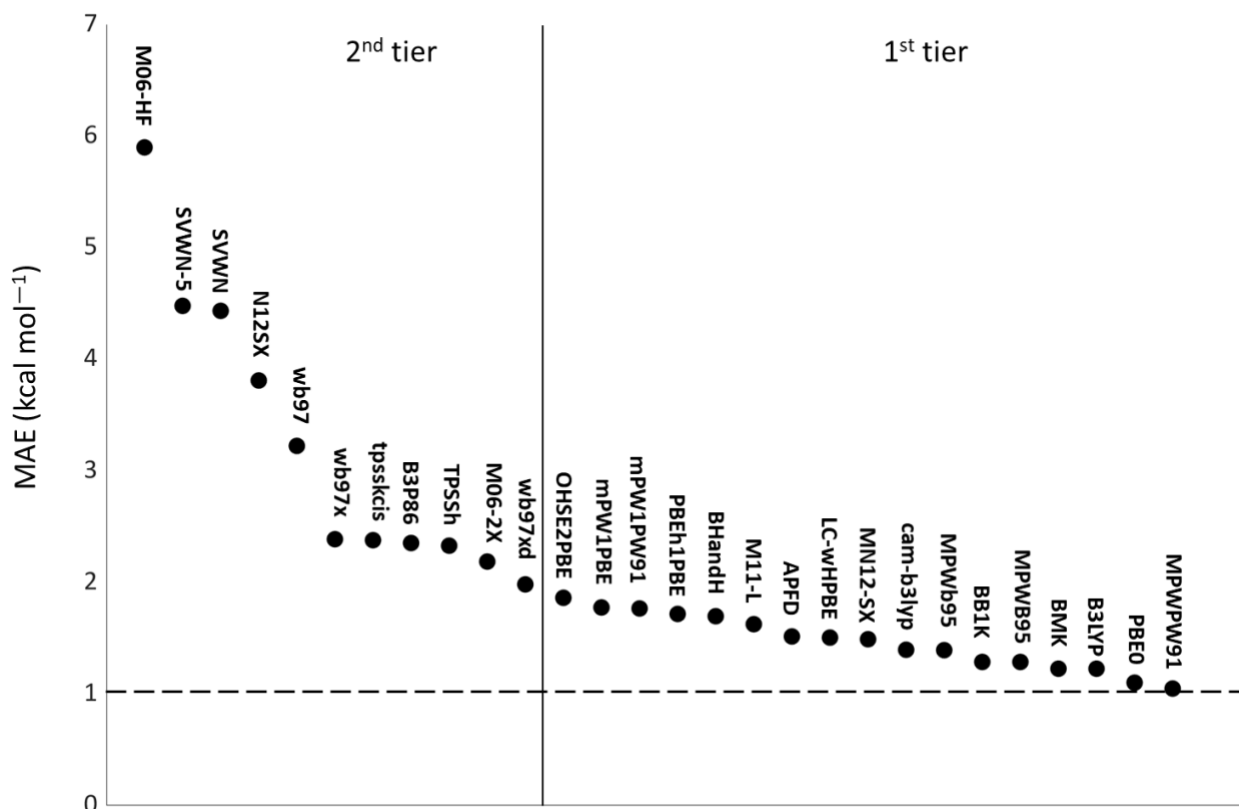


Figure 2. MAE values for each functional with the 6-311+G(d,p) basis set and the two accuracy tiers observed for tested functionals. The MAEs in the first tier are all below 2.0 kcal mol⁻¹, and the MAEs in the second tier are above 2.0 kcal mol⁻¹. The dotted black line represents the cutoff of chemical accuracy (1.0 kcal mol⁻¹).

Both LSDA functionals (SVWN and SVWN-5) are among the highest MAEs (4.4 and 4.5 kcal mol⁻¹, respectively). The LSDA exchange was developed to approximate HF-exchange. However, because it was derived from the HF-density matrix constructed with the plane wave orbitals of the uniform electron gas, the LSDA exchange functional typically underestimates the exchange energy by 10–15% for inhomogeneous many-electron systems,^{44, 103} such as azoarenes.

The range separated functionals (N12-SX, ω B97, ω B97X, and ω B97XD) were all present in the 2nd tier, with ω B97 giving the highest MAE (3.2 kcal mol⁻¹). The standard long-range correction of range separated functionals features a two-electron operator that is separated into the short-range and long-range parts, where conventionally the short-range part is described with GGA, while long-range is described with HF-exchange integral.^{104, 105} The relatively poor performance of all considered range separated functionals is a result of long-range corrected functionals being parameterized in a way that allows for correcting the long-range charge transfer errors in Time-Dependent DFT without contaminating the short-range part of exchange-correlation potential with extra HF-exchange. Such choice is motivated by the observation that

only full HF-exchange properly describes the distance dependence of long-range charge-transfer excitation energies. However, Rohrdanz and Herberta showed that a single range-separation parameter could not provide reasonable accuracy in the prediction of both ground-state properties and vertical excitation energies. As stated by the authors, the reasonable errors in atomization energies and barrier heights are achieved only at the expense of excessively high excitation energies and vice versa.¹⁰⁶

The two global hybrid-GGA functionals that belong to tier 2 and perform poorly relative to the other global hybrids are M06-2X (2.2 kcal mol⁻¹) and M06-HF (5.9 kcal mol⁻¹). The connection between these functionals is the high percentage of Hartree-Fock HF-exchange as compared to the other global hybrids that performed well. To explore the effects of HF-exchange on MAE, we evaluated five hybrid functionals that do not contain dispersion corrections (M06-2X, M06-HF, BHandH, PBEh1PBE, and mPW1PW91). The PBEh1PBE and mPW1PW91 functionals have 25% HF-exchange, while the BhandH, M06-2X, and M06-HF have 50%, 54%, and 100% of HF-exchange, respectively.

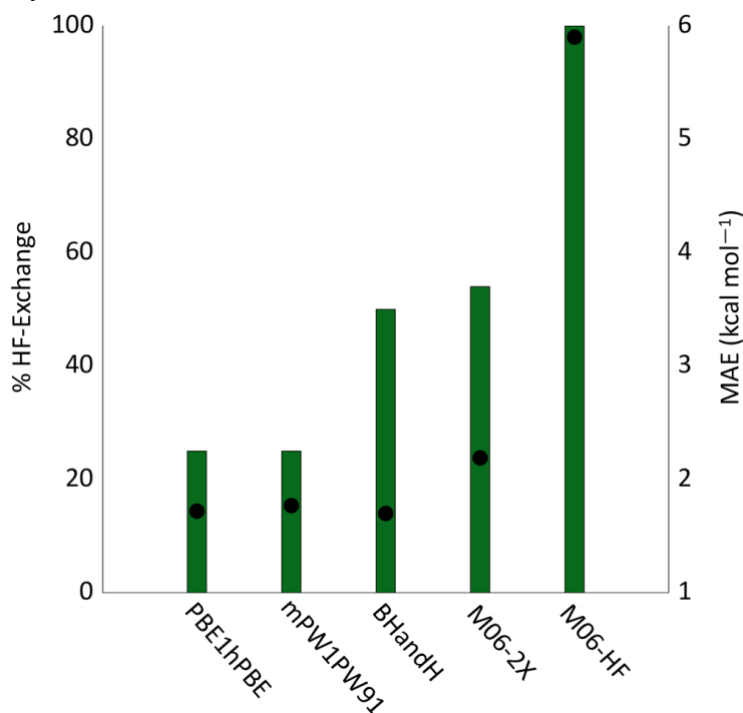


Figure 3. MAE for five hybrid functionals as a function of Hartree-Fock exchange. MAEs are evaluated for the 6-311+G(d,p) basis set. The green bars represent the amount of HF-exchange in each functional, and the black dots represent the MAE in kcal mol⁻¹.

The PBEh1PBE and mPW1PW91 functionals both contain 25% HF-exchange and have MAE values of 1.7 and 1.8 kcal mol⁻¹, respectively. From there, the MAEs generally increase along with the amount of HF-exchange. The only exception to this is the BHandH functional, which contains 50% HF-exchange, and has an MAE of 1.7 kcal mol⁻¹. As the amount of HF-exchange is increased to 54% in the M06-2X functional, the MAE increased significantly by 0.5 kcal mol⁻¹ (2.2 kcal mol⁻¹). Finally, the M06-HF functional (100% HF-exchange) had an MAE of 5.9 kcal mol⁻¹,

indicating that the large increase of HF-exchange causes a significant increase in MAEs. This was also the result found in 2017 by Rietze and co-workers, where the exchange-only HF-method gave the largest error in predicting azobenzene thermal reaction kinetics (5.0 kcal mol⁻¹). Moreover, Brothers and coworkers have shown computationally that a large percentage of HF-exchange contribute to increasing error for reactions where there is a rehybridization of bonds in the transition state.¹⁰⁷

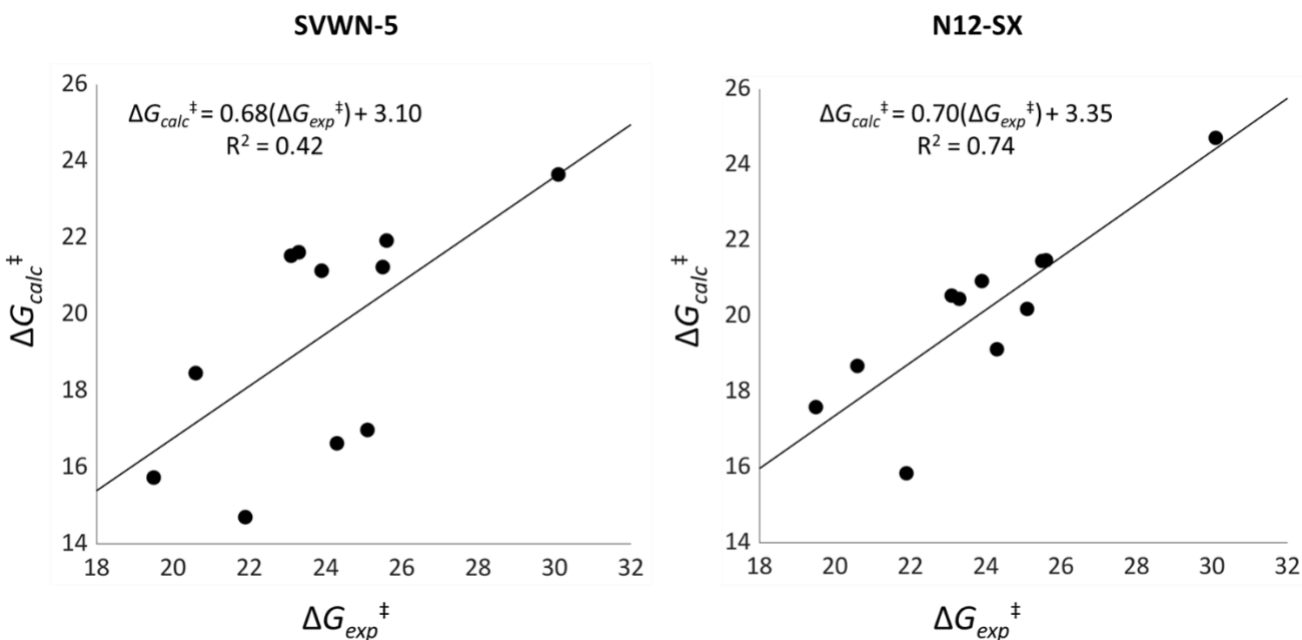
We now move to an analysis of the first tier (MAEs of 1.9 kcal mol⁻¹ and below) of functional performance. The best performing functionals in this tier approached chemical accuracy (1.0 kcal mol⁻¹) for predicting azoarene thermal isomerization barriers. Some functionals included here are CAM-B3LYP, LC-wHPBE, MN12-SX, and M11-L. As mentioned earlier the MN12-SX functional performs well (MAE of 1.5 kcal mol⁻¹) because this functional is a range separated meta-GGA functional that uses screened exchange (SX) version of range separation, which allows it to overcome the compromise between the accuracy of prediction of excited states energies and ground state barriers that arise for conventional long-range corrected range separated functionals. The LC-wHPBE functional provides accurate MAE (1.5 kcal mol⁻¹). This functional has a lower percentage (20%) of long-range correction compared to other range separated functionals. Although CAM-B3LYP has a high percentage (33%) of long-range correction, the reasonable performance of this functional in predicting reaction barriers was demonstrated before in a study by Handy and coworkers where they demonstrated that MAE obtained for BH42/04 dataset⁷⁴ is as low as 2.1 kcal mol⁻¹, which is in agreement with MAE of 1.4 kcal mol⁻¹ obtained in the present study. The relatively low MAE of 1.6 kcal mol⁻¹ calculated with M11-L is most likely due to the high parametrization of this functional compared to the other functionals and the rest of the functionals in the Minnesota family. The M11-L functional has 49 parameters, while B3LYP, ω B97X, M05, M06, and M08-HX functionals have 3, 14, 22, 38, and 44 parameters, respectively.⁶⁹

Other functionals that are in the top tier are PBE0, PBEh1PBE, OHSE2PBE, mPW1PBE, mPW1PW91, mPWPW91, and B3LYP. Hybrid meta-GGA functionals of MPW and MPW1 type are among the best performing functionals, with a range of calculated MAEs between 1.0-1.8 kcal mol⁻¹. These results are supported by the work of Zhao and Truhlar in which they demonstrated that MPW1B95 and MPWB1K total mean unsigned errors (TMUE) for thermochemistry of multiple test sets (AE109/3 atomization energy database,¹⁰⁸ BH42/04 barrier height database,⁷⁴ AE6 representative atomization energy database,¹⁰⁹ BH6 representative barrier height database,¹⁰⁹ SPG15/02 saddle point geometries database,¹¹⁰ ZPE13/99 zero-point energy database,¹¹¹ HB4/04 hydrogen bonding database, WI4/04 weak interaction database) are as low as 1.2 and 1.7 kcal mol⁻¹, respectively.⁷⁰ Finally, the class of functionals that performs consistently well in this study are the global hybrid GGA functionals which include PBE0, PBEh1PBE, OHSE2PBE, B3P86, and B3LYP.

The trends established in this study show that the meta-GGA density functionals afford relatively low MAEs (1.4–1.6 kcal mol⁻¹), with M06-2X, TPSSh, and TPSS1KCIS being exceptions (2.2, 2.3, and 2.4 kcal mol⁻¹, respectively). The M06-2X functional contains 54% HF-exchange, whereas the other surveyed meta-GGA functionals contain 42% (BB1K), 25% (MN12-

SX), and 0% (M11-L and TPSS1KCIS). This also aligns with the effects of HF-exchange that were established in global hybrid GGA functionals utilized in this study (Figure 3). LSDA functionals, along with functionals containing a high percentage of HF-exchange, gave high MAEs. We also found that the range separated functionals afforded relatively large errors. GGA functionals also generally gave lower MAEs than meta-GGA functionals. All of these results are for the 6-311+G(d,p) basis set, and the results follow similar trends for the other basis sets (6-31G(d), 6-31+G(d,p), cc-pvdz, and aug-cc-pvdz).

Next, we evaluate the performance of our functionals and basis sets in predicting the reactivity of azoarenes used for this study. The purpose of this analysis was to compare the ability of the functionals to measure the relative reactivity of photoswitches. Figure 4 shows the top-performing functionals for each of the first four rungs on Jacob's ladder, and their computed and experimentally measured ΔG^\ddagger values. The lines of best fit are presented on each graph, along with their equations, and R^2 values.



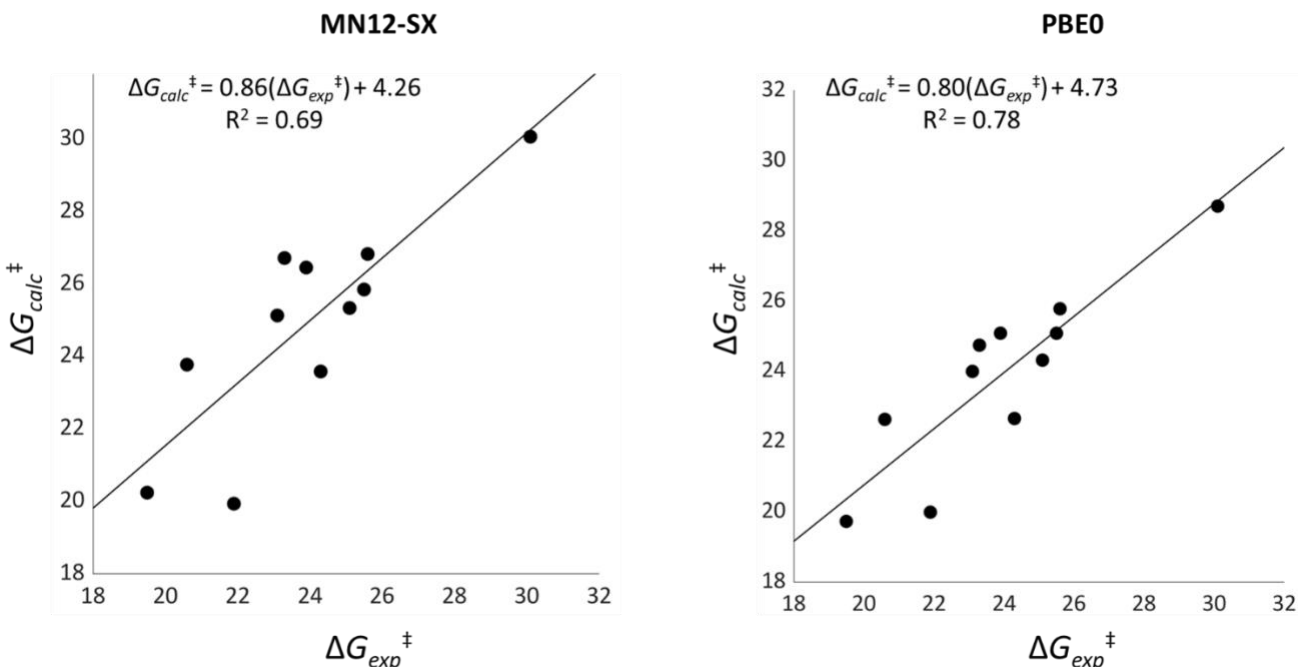


Figure 4. Experimental vs. theoretical half-life comparison of photoswitches benchmarked in this study. We've included SVWN-5 (LSDA functional, top-left), N12-SX(GGA-functional, top-right), MN12-SX (meta-GGA functional, bottom-left), and PBE0 (global hybrid functional, bottom-right). The lines on each graph represent the line of best fit.

Of the top-performing functionals from each rung on Jacob's Ladder, the SVWN-5 LSDA functional (first rung) had the worst performance in predicting azoarene reactivity, with an R^2 value of 0.42. The N12-SX GGA functional (second rung) offered a large performance improvement, with an R^2 value of 0.74. The MN12-SX meta-GGA functional (third rung) performed worse in predicting azoarene reactivity than the N12-SX GGA functional, giving an R^2 value of 0.69. This result contrasts the improvement in MAE of the MN12-SX functional over N12-SX. The PBE0 density functional (fourth rung) had the best overall performance, giving an R^2 value of 0.78. This functional also gave the best overall performance with respect to MAE. We assessed the qualitative performance of the PBE0 functional to determine if adding diffuse functions to the basis set would improve performance. Figure 5 shows the experimental vs. theoretical half-life comparison for the PBE0 functional with the 6-31G(d), 6-31+G(d,p), cc-pvdz, and aug-cc-pvdz basis sets.

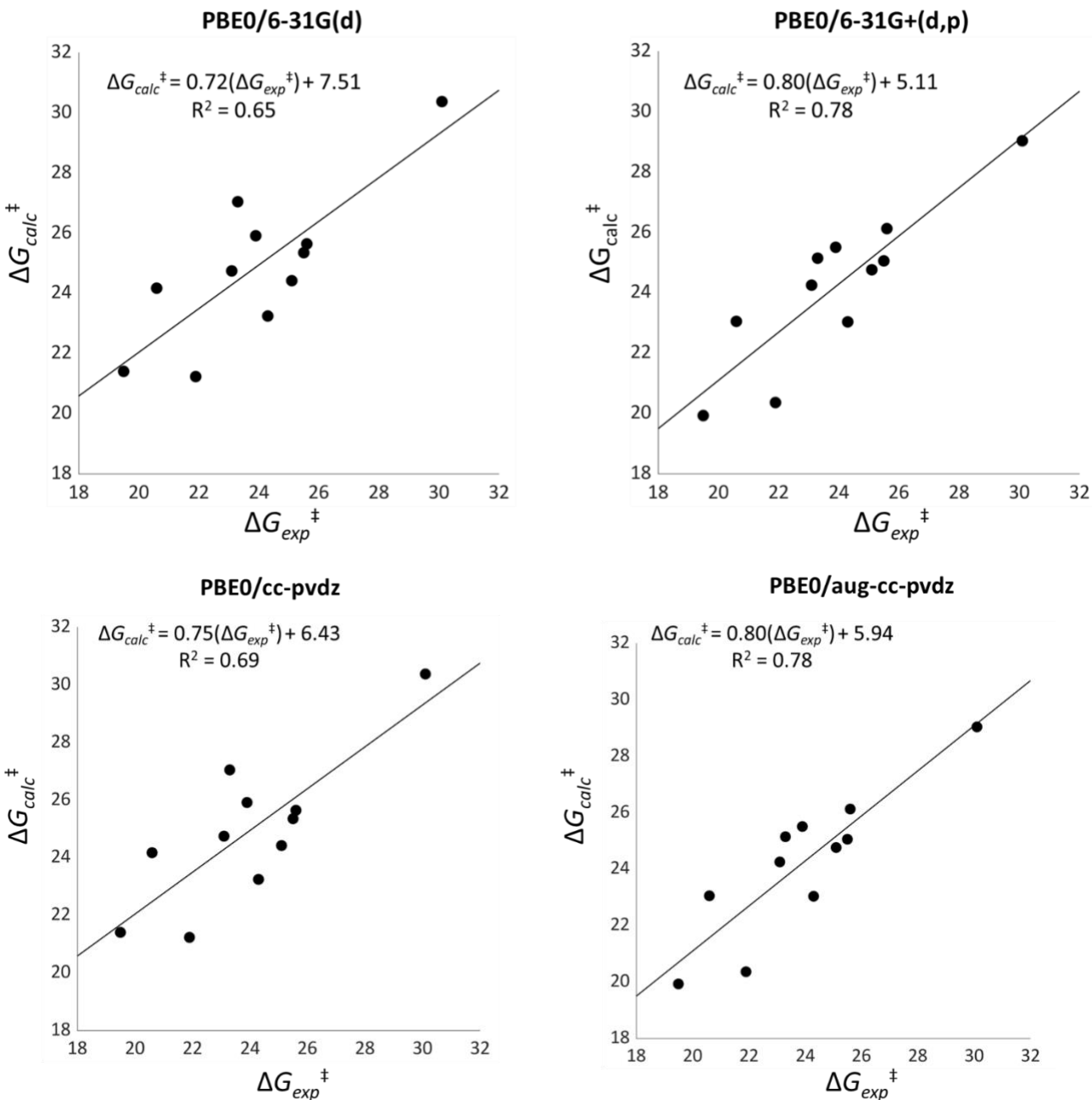


Figure 5. Experimental vs. theoretical half-life comparison of azoarene photoswitches benchmarked in this study. The graphs represent the best performing functional, PBE0, used with the 6-31G(d) (top left), 6-31+G(d,p) (top right), cc-pvdz (bottom left), and aug-cc-pvdz (bottom right) basis sets. The lines on each graph represent the lines of best fit.

Figure 5 shows the basis set effects on the performance of PBE0 in predicting azoarene photoswitch reactivity. We first assess the Pople basis sets (top row). The 6-31G(d) basis set performed the worst in predicting reactivity with an R^2 value of 0.65. The 6-31+G(d,p) basis set, which adds diffuse functions, offered a significant improvement over 6-31G(d), with an R^2 of 0.78.

The 6-311+G(d,p) triple- ζ basis set (Figure 4) performed identically to the 6-31+G(d,p) basis set, giving an R^2 of 0.78. Next, we examine the correlation consistent basis sets cc-pvdz and aug-cc-pvdz. The cc-pvdz basis set had an R^2 value of 0.71. The aug-cc-pvdz basis set adds diffuse functions to cc-pvdz, and offers an improvement, with an R^2 value of 0.78 compared to 0.71. This value is on par with the 6-31+G(d,p) and 6-311+G(d,p) basis sets. We then compared the performance of the model chemistries which gave the lowest 10% of MAEs with respect to the computational times for the frequency calculation of the transition structures (Figure 6).

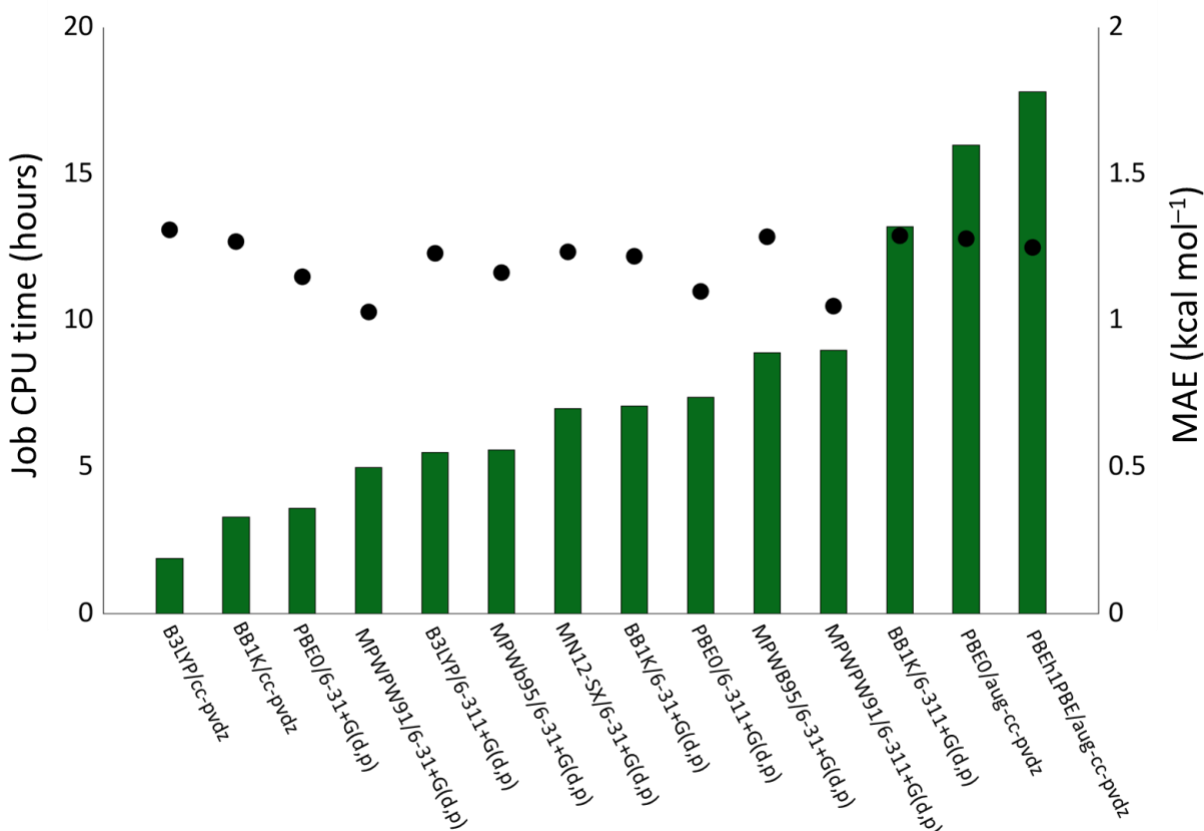


Figure 6. Top 14 performing model chemistries for ΔG_{comp}^\ddagger . The green bars represent the wall CPU time to complete a vibrational frequency analysis of the transition structures (in hours), and the black dots represent the MAE for a given model chemistry in kcal mol.

We further examined this set of 14 model chemistries because they had the lowest MAEs across all 140 computational methods. The range of MAE values in this subset is 0.3 kcal mol⁻¹. The mPWPW91/6-31+G(d,p) model chemistry gave the lowest MAE value overall (1.0 kcal mol⁻¹). The highest MAE (1.3 kcal mol⁻¹) of these top-performing methods corresponds to B3LYP/cc-pvdz. Four of the five basis sets (6-31+G(d,p), 6-311+G(d,p), cc-pvdz, and aug-cc-pvdz) and eight of the 28 functionals (PBEh1PBE, BB1K, mPWPW91, PBE0, B3LYP, MPWB95, MPWb95, and MN12-SX) used in our study are represented in the lowest 10%. The green bars represent the average CPU time for the frequency calculation for each respective model chemistry, ordered from

fastest to slowest along the x-axis. The black dots represent the average MAE for each model chemistry in kcal mol⁻¹. The shortest average time of 1.9 hours was for the B3LYP/cc-pvdz model chemistry. The longest average time of 17.8 hours was for the PBEh1PBE/aug-cc-pvdz model chemistry. The three shortest average CPU times (1.9 - 3.6 hours) were for model chemistries including the cc-pvdz and 6-31+G(d,p) basis sets. The seven longest average CPU times (7.1 hours – 17.8 hours) were all for model chemistries including the 6-311+G(d,p) or aug-cc-pvdz basis sets. The model chemistry with the lowest average MAE (mPWPW91/6-31+G(d,p)) had an average CPU time of just 5 hours, one of the lowest times out of all 14 model chemistries depicted in Figure 6. We conclude that while adding diffuse functions to increase basis set size or adding triple- ζ functions can afford a slightly more accurate model chemistry, the computational cost grows exponentially.

Conclusion

We provide an automatic framework (EZ-TS) to handle 1000s of quantum mechanical computations towards predicting azoarene $Z \rightarrow E$ isomerization activation free energies. We have performed a benchmarking of 28 density functionals and 5 basis sets for predicting the $\Delta G_{\text{expt}}^{\ddagger}$. We included LSDA-type functionals, GGA-functionals, meta-GGA functionals, and hybrid functionals with diffuse functions, double- ζ , and triple- ζ basis sets (Pople and correlation-consistent). We compared our $\Delta G_{\text{comp}}^{\ddagger}$ with $\Delta G_{\text{expt}}^{\ddagger}$ and calculated the MAE for each model chemistry and molecule. The MAEs ranged from 1.0 kcal mol (PBEh1PBE/aug-cc-pvdz) to 7.0 kcal mol (M06-HF/6-31G(d)). The hybrid functionals afforded the lowest MAEs out of all that were tested, The PBE0 functional with the 6-31+G(d,p), 6-311+G(d,p), and aug-cc-pvdz basis sets best predicted the relative azoarene reactivity (R^2 value of 0.78). We identified 14 model chemistries that approach chemical accuracy with MAEs ranging from 1.0-1.3 kcal mol⁻¹, with the mPWPW91/6-31+G(d,p) model chemistry giving the lowest MAE (1.0 kcal mol⁻¹). The range within the set of lowest 14 model chemistries was small (0.3 kcal mol⁻¹), indicating that any of them would be adequate in predicting $\Delta G_{\text{expt}}^{\ddagger}$. With our most accurate model chemistries, we were able to predict azoarene $Z \rightarrow E$ activation barriers within a single order of magnitude and accurately predict the thermal reactivity of the meta-stable azoarene Z isomers. An analysis of the frequency calculation job times for the best performing model chemistries also indicated that using basis sets containing diffuse and triple- ζ basis functions increased the computational time by nearly tenfold, while only offering a relatively small (0.30 kcal mol⁻¹) improvement in MAEs.

References

1. Jones, I. M.; Lingard, H.; Hamilton, A. D., pH-dependent conformational switching in 2,6-benzamidodiphenylacetylenes. *Angew Chem Int Ed Engl* **2011**, *50* (52), 12569-71.
2. Leblond, J.; Gao, H.; Petitjean, A.; Leroux, J. C., pH-Responsive molecular tweezers. *J Am Chem Soc* **2010**, *132* (25), 8544-5.
3. Muraoka, M.; Irie, H.; Nakatsuji, Y., Acid/base controllable molecular switch based on a neutral phenanthroline guest penetrated pseudorotaxane. *Org Biomol Chem* **2010**, *8* (10), 2408-13.

4. Landge, S. M.; Aprahamian, I., A pH activated configurational rotary switch: controlling the E/Z isomerization in hydrazones. *J Am Chem Soc* **2009**, *131* (51), 18269-71.
5. Brazdova, B.; Zhang, N.; Samoshin, V. V.; Guo, X., trans-2-Aminocyclohexanol as a pH-sensitive conformational switch in lipid amphiphiles. *Chem Commun (Camb)* **2008**, (39), 4774-6.
6. Tuncel, D.; Katterle, M., pH-Triggered dethreading-rethreading and switching of cucurbit[6]uril on bistable [3]pseudorotaxanes and [3]rotaxanes. *Chemistry* **2008**, *14* (13), 4110-6.
7. Walkey, M. C.; Peiris, C. R.; Ciampi, S.; A, C. A.; Dominguez-Espindola, R. B.; Jago, D.; Pulbrook, T.; Skelton, B. W.; Sobolev, A. N.; Diez Perez, I.; Piggott, M. J.; Koutsantonis, G. A.; Darwish, N., Chemically and Mechanically Controlled Single-Molecule Switches Using Spiropyran. *ACS Appl Mater Interfaces* **2019**, *11* (40), 36886-36894.
8. Zhang, Y.; Ma, Y.; Sun, J., Reversible actuation of polyelectrolyte films: expansion-induced mechanical force enables cis-trans isomerization of azobenzenes. *Langmuir* **2013**, *29* (48), 14919-25.
9. Zhou, H.-Y.; Han, Y.; Shi, Q.; Chen, C.-F., A Triply Operable Molecular Switch: Anion-, Acid/Base- and Solvent-Responsive [2]Rotaxane. *European Journal of Organic Chemistry* **2019**, *2019* (21), 3406-3411.
10. Bleger, D.; Hecht, S., Visible-Light-Activated Molecular Switches. *Angew Chem Int Ed Engl* **2015**, *54* (39), 11338-49.
11. Petermayer, C.; Dube, H., Indigoid Photoswitches: Visible Light Responsive Molecular Tools. *Acc Chem Res* **2018**, *51* (5), 1153-1163.
12. Crespi, S.; Simeth, N. A.; König, B., Heteroaryl azo dyes as molecular photoswitches. *Nature Reviews Chemistry* **2019**, *3* (3), 133-146.
13. Fehrentz, T.; Schonberger, M.; Trauner, D., Optochemical genetics. *Angew Chem Int Ed Engl* **2011**, *50* (51), 12156-82.
14. Broichhagen, J.; Podewin, T.; Meyer-Berg, H.; von Ohlen, Y.; Johnston, N. R.; Jones, B. J.; Bloom, S. R.; Rutter, G. A.; Hoffmann-Roder, A.; Hodson, D. J.; Trauner, D., Optical Control of Insulin Secretion Using an Incretin Switch. *Angew Chem Int Ed Engl* **2015**, *54* (51), 15565-9.
15. Laprell, L.; Repak, E.; Franckevicius, V.; Hartrampf, F.; Terhag, J.; Hollmann, M.; Sumser, M.; Rebola, N.; DiGregorio, D. A.; Trauner, D., Optical control of NMDA receptors with a diffusible photoswitch. *Nat Commun* **2015**, *6*, 8076.
16. Hull, K.; Morstein, J.; Trauner, D., In Vivo Photopharmacology. *Chem Rev* **2018**, *118* (21), 10710-10747.
17. Tochitsky, I.; Kienzler, M. A.; Isacoff, E.; Kramer, R. H., Restoring Vision to the Blind with Chemical Photoswitches. *Chem Rev* **2018**, *118* (21), 10748-10773.
18. Albert, L.; Vazquez, O., Photoswitchable peptides for spatiotemporal control of biological functions. *Chem Commun (Camb)* **2019**, *55* (69), 10192-10213.
19. Hernandez, J. V.; Kay, E. R.; Leigh, D. A., A reversible synthetic rotary molecular motor. *Science* **2004**, *306* (5701), 1532-7.
20. Dattler, D.; Fuks, G.; Heiser, J.; Moulin, E.; Perrot, A.; Yao, X.; Giuseppone, N., Design of Collective Motions from Synthetic Molecular Switches, Rotors, and Motors. *Chem Rev* **2020**, *120* (1), 310-433.
21. Gerwien, A.; Mayer, P.; Dube, H., Green light powered molecular state motor enabling eight-shaped unidirectional rotation. *Nat Commun* **2019**, *10* (1), 4449.
22. Calbo, J.; Weston, C. E.; White, A. J.; Rzepa, H. S.; Contreras-Garcia, J.; Fuchter, M. J., Tuning Azoheteroarene Photoswitch Performance through Heteroaryl Design. *J Am Chem Soc* **2017**, *139* (3), 1261-1274.
23. Calbo, J.; Thawani, A. R.; Gibson, R. S. L.; White, A. J. P.; Fuchter, M. J., A combinatorial approach to improving the performance of azoarene photoswitches. *Beilstein J Org Chem* **2019**, *15*, 2753-2764.

24. Kortekaas, L.; Simke, J.; Kurka, D. W.; Ravoo, B. J., Rapid Photoswitching of Low Molecular Weight Arylazoisoxazole Adhesives. *ACS Appl Mater Interfaces* **2020**, *12* (28), 32054-32060.
25. Kumar, P.; Srivastava, A.; Sah, C.; Devi, S.; Venkataramani, S., Arylazo-3,5-dimethylisoxazoles: Azoheteroarene Photoswitches Exhibiting High Z-Isomer Stability, Solid-State Photochromism, and Reversible Light-Induced Phase Transition. *Chemistry* **2019**, *25* (51), 11924-11932.
26. Cechova, L.; Filo, J.; Dracinsky, M.; Slavov, C.; Sun, D.; Janeba, Z.; Slanina, T.; Wachtveitl, J.; Prochazkova, E.; Cigan, M., Polysubstituted 5-Phenylazopyrimidines: Extremely Fast Non-ionic Photochromic Oscillators. *Angew Chem Int Ed Engl* **2020**, *59* (36), 15590-15594.
27. Coelho, P. J.; Castro, M. C. R.; Fernandes, S. S. M.; Fonseca, A. M. C.; Raposo, M. M. M., Enhancement of the photochromic switching speed of bithiophene azo dyes. *Tetrahedron Letters* **2012**, *53* (34), 4502-4506.
28. Coelho, P. J.; Carvalho, L. M.; Moura, J. C. V. P.; Raposo, M. M. M., Novel photochromic 2,2'-bithiophene azo dyes. *Dyes and Pigments* **2009**, *82* (2), 130-133.
29. Jaunet-Lahary, T.; Chantzis, A.; Chen, K. J.; Laurent, A. D.; Jacquemin, D., Designing Efficient Azobenzene and Azothiophene Nonlinear Optical Photochromes. *The Journal of Physical Chemistry C* **2014**, *118* (49), 28831-28841.
30. Huddleston, P. R.; Volkov, V. V.; Perry, C. C., The structural and electronic properties of 3,3'-azothiophene photo-switching systems. *Phys Chem Chem Phys* **2019**, *21* (3), 1344-1353.
31. de Oliveira, R. B.; de Souza-Fagundes, E. M.; Siqueira, H. A.; Leite, R. S.; Donnici, C. L.; Zani, C. L., Synthesis and evaluation of cytotoxic activity of arylfurans. *Eur J Med Chem* **2006**, *41* (6), 756-60.
32. Slavov, C.; Yang, C.; Heindl, A. H.; Wegner, H. A.; Dreuw, A.; Wachtveitl, J., Thiophenylazobenzene: An Alternative Photoisomerization Controlled by Lone-Pairpi Interaction. *Angew Chem Int Ed Engl* **2020**, *59* (1), 380-387.
33. Heindl, A. H.; Wegner, H. A., Rational Design of Azothiophenes-Substitution Effects on the Switching Properties. *Chemistry* **2020**, *26* (60), 13730-13737.
34. Wang, Y.; Ma, J.; Jiang, Y., Tuning of electronic structures of poly(p-phenylenevinylene) analogues of phenyl, thienyl, furyl, and pyrrolyl by double-bond linkages of group 14 and 15 elements. *J Phys Chem A* **2005**, *109* (32), 7197-206.
35. Åstrand, P.-O.; Sommer-Larsen, P.; Hvilsted, S.; Ramanujam, P. S.; Bak, K. L.; Sauer, S. P. A., Five-membered rings as diazo components in optical data storage devices: an ab initio investigation of the lowest singlet excitation energies. *Chemical Physics Letters* **2000**, *325* (1-3), 115-119.
36. Crecca, C. R.; Roitberg, A. E., Theoretical study of the isomerization mechanism of azobenzene and disubstituted azobenzene derivatives. *J Phys Chem A* **2006**, *110* (26), 8188-203.
37. Muzdalo, A.; Saalfrank, P.; Vreede, J.; Santer, M., Cis-to- Trans Isomerization of Azobenzene Derivatives Studied with Transition Path Sampling and Quantum Mechanical/Molecular Mechanical Molecular Dynamics. *J Chem Theory Comput* **2018**, *14* (4), 2042-2051.
38. Dokic, J.; Gothe, M.; Wirth, J.; Peters, M. V.; Schwarz, J.; Hecht, S.; Saalfrank, P., Quantum chemical investigation of thermal cis-to-trans isomerization of azobenzene derivatives: substituent effects, solvent effects, and comparison to experimental data. *J Phys Chem A* **2009**, *113* (24), 6763-73.
39. Robertus, J.; Reker, S. F.; Pijper, T. C.; Deuzeman, A.; Browne, W. R.; Feringa, B. L., Kinetic analysis of the thermal isomerisation pathways in an asymmetric double azobenzene switch. *Phys Chem Chem Phys* **2012**, *14* (13), 4374-82.
40. Asano, T.; Okada, T.; Shinkai, S.; Shigematsu, K.; Kusano, Y.; Manabe, O., Temperature and pressure dependences of thermal cis-to-trans isomerization of azobenzenes

which evidence an inversion mechanism. *Journal of the American Chemical Society* **1981**, *103* (17), 5161-5165.

41. Rietze, C.; Titov, E.; Lindner, S.; Saalfrank, P., Thermal isomerization of azobenzenes: on the performance of Eyring transition state theory. *J Phys Condens Matter* **2017**, *29* (31), 314002.

42. Hertwig, R. H.; Koch, W., On the parameterization of the local correlation functional. What is Becke-3-LYP? *Chemical Physics Letters* **1997**, *268* (5-6), 345-351.

43. Grimme, S.; Ehrlich, S.; Goerigk, L., Effect of the damping function in dispersion corrected density functional theory. *J Comput Chem* **2011**, *32* (7), 1456-65.

44. Becke, A. D., Density-functional thermochemistry. III. The role of exact exchange. *The Journal of Chemical Physics* **1993**, *98* (7), 5648-5652.

45. Ditchfield, R.; Hehre, W. J.; Pople, J. A., Self-Consistent Molecular-Orbital Methods. IX. An Extended Gaussian-Type Basis for Molecular-Orbital Studies of Organic Molecules. *The Journal of Chemical Physics* **1971**, *54* (2), 724-728.

46. Biswas, N.; Umapathy, S., Density Functional Calculations of Structures, Vibrational Frequencies, and Normal Modes of trans- and cis-Azobenzene. *The Journal of Physical Chemistry A* **1997**, *101* (30), 5555-5566.

47. Mardirossian, N.; Head-Gordon, M., Thirty years of density functional theory in computational chemistry: an overview and extensive assessment of 200 density functionals. *Molecular Physics* **2017**, *115* (19), 2315-2372.

48. Peverati, R.; Truhlar, D. G., Quest for a universal density functional: the accuracy of density functionals across a broad spectrum of databases in chemistry and physics. *Philos Trans A Math Phys Eng Sci* **2014**, *372* (2011), 20120476.

49. Perdew, J. P.; Ruzsinszky, A.; Tao, J.; Staroverov, V. N.; Scuseria, G. E.; Csonka, G. I., Prescription for the design and selection of density functional approximations: more constraint satisfaction with fewer fits. *J Chem Phys* **2005**, *123* (6), 62201.

50. Perdew, J. P.; Constantin, L. A., Laplacian-level density functionals for the kinetic energy density and exchange-correlation energy. *Physical Review B* **2007**, *75* (15).

51. Schmider, H. L.; Becke, A. D., Chemical content of the kinetic energy density. *Journal of Molecular Structure: THEOCHEM* **2000**, *527* (1-3), 51-61.

52. Perdew, J. P.; McMullen, E. R.; Zunger, A., Density-functional theory of the correlation energy in atoms and ions: A simple analytic model and a challenge. *Physical Review A* **1981**, *23* (6), 2785-2789.

53. Becke, A. D., A new mixing of Hartree-Fock and local density-functional theories. *The Journal of Chemical Physics* **1993**, *98* (2), 1372-1377.

54. Adamo, C.; Barone, V., Toward reliable density functional methods without adjustable parameters: The PBE0 model. *The Journal of Chemical Physics* **1999**, *110* (13), 6158-6170.

55. Lee, C.; Yang, W.; Parr, R. G., Development of the Colle-Salvetti correlation-energy formula into a functional of the electron density. *Phys Rev B Condens Matter* **1988**, *37* (2), 785-789.

56. Vosko, S. H.; Wilk, L.; Nusair, M., Accurate spin-dependent electron liquid correlation energies for local spin density calculations: a critical analysis. *Canadian Journal of Physics* **1980**, *58* (8), 1200-1211.

57. Stephens, P. J.; Devlin, F. J.; Chabalowski, C. F.; Frisch, M. J., Ab Initio Calculation of Vibrational Absorption and Circular Dichroism Spectra Using Density Functional Force Fields. *The Journal of Physical Chemistry* **2002**, *98* (45), 11623-11627.

58. Boese, A. D.; Martin, J. M., Development of density functionals for thermochemical kinetics. *J Chem Phys* **2004**, *121* (8), 3405-16.

59. Austin, A.; Petersson, G. A.; Frisch, M. J.; Dobek, F. J.; Scalmani, G.; Throssell, K., A Density Functional with Spherical Atom Dispersion Terms. *J Chem Theory Comput* **2012**, *8* (12), 4989-5007.

60. Peverati, R.; Truhlar, D. G., Screened-exchange density functionals with broad accuracy for chemistry and solid-state physics. *Phys Chem Chem Phys* **2012**, *14* (47), 16187-91.
61. Zhao, Y.; Truhlar, D. G., The M06 suite of density functionals for main group thermochemistry, thermochemical kinetics, noncovalent interactions, excited states, and transition elements: two new functionals and systematic testing of four M06-class functionals and 12 other functionals. *Theoretical Chemistry Accounts* **2007**, *120* (1-3), 215-241.
62. Zhao, Y.; Truhlar, D. G., Density functional for spectroscopy: no long-range self-interaction error, good performance for Rydberg and charge-transfer states, and better performance on average than B3LYP for ground states. *J Phys Chem A* **2006**, *110* (49), 13126-30.
63. Ernzerhof, M.; Perdew, J. P., Generalized gradient approximation to the angle- and system-averaged exchange hole. *The Journal of Chemical Physics* **1998**, *109* (9), 3313-3320.
64. Heyd, J.; Scuseria, G. E.; Ernzerhof, M., Hybrid functionals based on a screened Coulomb potential. *The Journal of Chemical Physics* **2003**, *118* (18), 8207-8215.
65. Adamo, C.; Barone, V., Exchange functionals with improved long-range behavior and adiabatic connection methods without adjustable parameters: The mPW and mPW1PW models. *The Journal of Chemical Physics* **1998**, *108* (2), 664-675.
66. Yanai, T.; Tew, D. P.; Handy, N. C., A new hybrid exchange–correlation functional using the Coulomb-attenuating method (CAM-B3LYP). *Chemical Physics Letters* **2004**, *393* (1-3), 51-57.
67. Chai, J. D.; Head-Gordon, M., Long-range corrected hybrid density functionals with damped atom-atom dispersion corrections. *Phys Chem Chem Phys* **2008**, *10* (44), 6615-20.
68. Henderson, T. M.; Izmaylov, A. F.; Scalmani, G.; Scuseria, G. E., Can short-range hybrids describe long-range-dependent properties? *J Chem Phys* **2009**, *131* (4), 044108.
69. Peverati, R.; Truhlar, D. G., M11-L: A Local Density Functional That Provides Improved Accuracy for Electronic Structure Calculations in Chemistry and Physics. *The Journal of Physical Chemistry Letters* **2011**, *3* (1), 117-124.
70. Zhao, Y.; Truhlar, D. G., Hybrid Meta Density Functional Theory Methods for Thermochemistry, Thermochemical Kinetics, and Noncovalent Interactions: The MPW1B95 and MPWB1K Models and Comparative Assessments for Hydrogen Bonding and van der Waals Interactions. *The Journal of Physical Chemistry A* **2004**, *108* (33), 6908-6918.
71. Perdew, J. P.; Burke, K.; Ernzerhof, M., Generalized Gradient Approximation Made Simple. *Phys Rev Lett* **1996**, *77* (18), 3865-3868.
72. Zhao, Y.; Lynch, B. J.; Truhlar, D. G., Multi-coefficient extrapolated density functional theory for thermochemistry and thermochemical kinetics. *Physical Chemistry Chemical Physics* **2005**, *7* (1).
73. Lynch, B. J.; Fast, P. L.; Harris, M.; Truhlar, D. G., Adiabatic Connection for Kinetics. *The Journal of Physical Chemistry A* **2000**, *104* (21), 4811-4815.
74. Zhao, Y.; Lynch, B. J.; Truhlar, D. G., Development and Assessment of a New Hybrid Density Functional Model for Thermochemical Kinetics. *The Journal of Physical Chemistry A* **2004**, *108* (14), 2715-2719.
75. Becke, A. D., Density-functional exchange-energy approximation with correct asymptotic behavior. *Phys Rev A Gen Phys* **1988**, *38* (6), 3098-3100.
76. Chai, J. D.; Head-Gordon, M., Systematic optimization of long-range corrected hybrid density functionals. *J Chem Phys* **2008**, *128* (8), 084106.
77. Tao, J.; Perdew, J. P.; Staroverov, V. N.; Scuseria, G. E., Climbing the density functional ladder: nonempirical meta-generalized gradient approximation designed for molecules and solids. *Phys Rev Lett* **2003**, *91* (14), 146401.
78. Slater, J. C.; Phillips, J. C., Quantum Theory of Molecules and Solids Vol. 4: The Self-Consistent Field for Molecules and Solids. *Physics Today* **1974**, *27* (12), 49-50.

79. Woon, D. E.; Dunning, T. H., Gaussian basis sets for use in correlated molecular calculations. V. Core-valence basis sets for boron through neon. *The Journal of Chemical Physics* **1995**, *103* (11), 4572-4585.
80. Kendall, R. A.; Dunning, T. H.; Harrison, R. J., Electron affinities of the first-row atoms revisited. Systematic basis sets and wave functions. *The Journal of Chemical Physics* **1992**, *96* (9), 6796-6806.
81. Feller, D.; Dixon, D. A., Density Functional Theory and the Basis Set Truncation Problem with Correlation Consistent Basis Sets: Elephant in the Room or Mouse in the Closet? *J Phys Chem A* **2018**, *122* (9), 2598-2603.
82. Ranasinghe, D. S.; Petersson, G. A., CCSD(T)/CBS atomic and molecular benchmarks for H through Ar. *J Chem Phys* **2013**, *138* (14), 144104.
83. Martin, J. M. L., On the performance of correlation consistent basis sets for the calculation of total atomization energies, geometries, and harmonic frequencies. *The Journal of Chemical Physics* **1994**, *100* (11), 8186-8193.
84. Sylvetsky, N.; Kesharwani, M. K.; Martin, J. M. L., The aug-cc-pVnZ-F12 basis set family: Correlation consistent basis sets for explicitly correlated benchmark calculations on anions and noncovalent complexes. *J Chem Phys* **2017**, *147* (13), 134106.
85. Tomasi, J.; Mennucci, B.; Cammi, R., Quantum mechanical continuum solvation models. *Chem Rev* **2005**, *105* (8), 2999-3093.
86. Frisch, M. J.; Trucks, G. W.; Schlegel, H. B.; Scuseria, G. E.; Robb, M. A.; Cheeseman, J. R.; Scalmani, G.; Barone, V.; Petersson, G. A.; Nakatsuji, H.; Li, X.; Caricato, M.; Marenich, A. V.; Bloino, J.; Janesko, B. G.; Gomperts, R.; Mennucci, B.; Hratchian, H. P.; Ortiz, J. V.; Izmaylov, A. F.; Sonnenberg, J. L.; Williams, D.; Ding, F.; Lipparini, F.; Egidi, F.; Goings, J.; Peng, B.; Petrone, A.; Henderson, T.; Ranasinghe, D.; Zakrzewski, V. G.; Gao, J.; Rega, N.; Zheng, G.; Liang, W.; Hada, M.; Ehara, M.; Toyota, K.; Fukuda, R.; Hasegawa, J.; Ishida, M.; Nakajima, T.; Honda, Y.; Kitao, O.; Nakai, H.; Vreven, T.; Throssell, K.; Montgomery Jr., J. A.; Peralta, J. E.; Ogliaro, F.; Bearpark, M. J.; Heyd, J. J.; Brothers, E. N.; Kudin, K. N.; Staroverov, V. N.; Keith, T. A.; Kobayashi, R.; Normand, J.; Raghavachari, K.; Rendell, A. P.; Burant, J. C.; Iyengar, S. S.; Tomasi, J.; Cossi, M.; Millam, J. M.; Klene, M.; Adamo, C.; Cammi, R.; Ochterski, J. W.; Martin, R. L.; Morokuma, K.; Farkas, O.; Foresman, J. B.; Fox, D. J. *Gaussian 16 Rev. C.01*, Wallingford, CT, 2016.
87. Heindl, A. H.; Wende, R. C.; Wegner, H. A., London dispersion as important factor for the stabilization of (Z)-azobenzenes in the presence of hydrogen bonding. *Beilstein J Org Chem* **2018**, *14*, 1238-1243.
88. Li, G.; Ma, X.; Jia, C.; Han, Q.; Wang, Y.; Wang, J.; Yu, L.; Yang, S., Ruthenium-catalyzed meta/ortho-selective C-H alkylation of azoarenes using alkyl bromides. *Chem Commun (Camb)* **2017**, *53* (7), 1261-1264.
89. Powers, I. G.; Andjaba, J. M.; Luo, X.; Mei, J.; Uyeda, C., Catalytic Azoarene Synthesis from Aryl Azides Enabled by a Dinuclear Ni Complex. *J Am Chem Soc* **2018**, *140* (11), 4110-4118.
90. Vela, S.; Scheidegger, A.; Fabregat, R.; Corminboeuf, C., Tuning the Thermal Stability and Photoisomerization of Azoheteroarenes through Macrocyclic Strain*. *Chemistry* **2021**, *27* (1), 419-426.
91. Slavov, C.; Yang, C.; Heindl, A. H.; Stauch, T.; Wegner, H. A.; Dreuw, A.; Wachtveitl, J., Twist and Return-Induced Ring Strain Triggers Quick Relaxation of a (Z)-Stabilized Cyclobisazobenzene. *J Phys Chem Lett* **2018**, *9* (16), 4776-4781.
92. Bassotti, E.; Carbone, P.; Credi, A.; Di Stefano, M.; Masiero, S.; Negri, F.; Orlandi, G.; Spada, G. P., Effect of strain on the photoisomerization and stability of a congested azobenzenophane: a combined experimental and computational study. *J Phys Chem A* **2006**, *110* (45), 12385-94.

93. Cramer, C. J.; Truhlar, D. G., Density functional theory for transition metals and transition metal chemistry. *Phys Chem Chem Phys* **2009**, *11* (46), 10757-816.
94. Qi, S.-C.; Hayashi, J.-i.; Zhang, L., Recent application of calculations of metal complexes based on density functional theory. *RSC Advances* **2016**, *6* (81), 77375-77395.
95. Weininger, D., SMILES, a chemical language and information system. 1. Introduction to methodology and encoding rules. *Journal of Chemical Information and Modeling* **1988**, *28* (1), 31-36.
96. Pracht, P.; Bohle, F.; Grimme, S., Automated exploration of the low-energy chemical space with fast quantum chemical methods. *Phys Chem Chem Phys* **2020**, *22* (14), 7169-7192.
97. Bannwarth, C.; Ehlert, S.; Grimme, S., GFN2-xTB-An Accurate and Broadly Parametrized Self-Consistent Tight-Binding Quantum Chemical Method with Multipole Electrostatics and Density-Dependent Dispersion Contributions. *J Chem Theory Comput* **2019**, *15* (3), 1652-1671.
98. Neese, F., The ORCA program system. *WIREs Computational Molecular Science* **2011**, *2* (1), 73-78.
99. Ingman, V. M.; Schaefer, A. J.; Andreola, L. R.; Wheeler, S. E., QChASM : Quantum chemistry automation and structure manipulation. *WIREs Computational Molecular Science* **2020**.
100. Bhoorasingh, P. L.; Slakman, B. L.; Seyedzadeh Khanshan, F.; Cain, J. Y.; West, R. H., Automated Transition State Theory Calculations for High-Throughput Kinetics. *J Phys Chem A* **2017**, *121* (37), 6896-6904.
101. Abreha, B. G.; Agarwal, S.; Foster, I.; Blaiszik, B.; Lopez, S. A., Virtual Excited State Reference for the Discovery of Electronic Materials Database: An Open-Access Resource for Ground and Excited State Properties of Organic Molecules. *J Phys Chem Lett* **2019**, *10* (21), 6835-6841.
102. Luchini, G.; Alegre-Requena, J. V.; Funes-Ardoiz, I.; Paton, R. S., GoodVibes: automated thermochemistry for heterogeneous computational chemistry data. *F1000Research* **2020**, *9*.
103. Kang, J. K.; Musgrave, C. B., Prediction of transition state barriers and enthalpies of reaction by a new hybrid density-functional approximation. *The Journal of Chemical Physics* **2001**, *115* (24), 11040-11051.
104. Iikura, H.; Tsuneda, T.; Yanai, T.; Hirao, K., A long-range correction scheme for generalized-gradient-approximation exchange functionals. *The Journal of Chemical Physics* **2001**, *115* (8), 3540-3544.
105. Adamson, R. D.; Dombroski, J. P.; Gill, P. M. W., Efficient calculation of short-range Coulomb energies. *Journal of Computational Chemistry* **1999**, *20* (9), 921-927.
106. Rohrdanz, M. A.; Herbert, J. M., Simultaneous benchmarking of ground- and excited-state properties with long-range-corrected density functional theory. *J Chem Phys* **2008**, *129* (3), 034107.
107. Mahler, A.; Janesko, B. G.; Moncho, S.; Brothers, E. N., When Hartree-Fock exchange admixture lowers DFT-predicted barrier heights: Natural bond orbital analyses and implications for catalysis. *J Chem Phys* **2018**, *148* (24), 244106.
108. Lynch, B. J.; Truhlar, D. G., Robust and Affordable Multicoefficient Methods for Thermochemistry and Thermochemical Kinetics: The MCCM/3 Suite and SAC/3. *The Journal of Physical Chemistry A* **2003**, *107* (19), 3898-3906.
109. Lynch, B. J.; Truhlar, D. G., Small Representative Benchmarks for Thermochemical Calculations. *The Journal of Physical Chemistry A* **2003**, *107* (42), 8996-8999.
110. Lynch, B. J.; Truhlar, D. G., What Are the Best Affordable Multi-Coefficient Strategies for Calculating Transition State Geometries and Barrier Heights? *The Journal of Physical Chemistry A* **2002**, *106* (5), 842-846.
111. Fast, P. L.; Corchado, J.; Sanchez, M. L.; Truhlar, D. G., Optimized Parameters for Scaling Correlation Energy. *The Journal of Physical Chemistry A* **1999**, *103* (17), 3139-3143.

TOC Graphic

